Journal of Mathematical Biology (2026) 93:45
https://doi.org/10.1007/s00285-026-02455-6

Mathematical Biology

To trace or not to trace: analytical insights from network-based contact-tracing models

Giulia de Meijere[1] · Andrea Pugliese[2] · Gerardo Iñiguez[1,3] · Péter L. Simon[4] · István Z. Kiss[5,6]

Received: 4 March 2026 / Revised: 17 June 2026 / Accepted: 11 August 2026
© The Author(s) 2026

Abstract

Contact tracing is one of the most important control measures deployed during epidemics and pandemics, relying on the identification of contacts of known infected individuals. A network perspective is therefore essential for its accurate modelling. Pairwise models have been used extensively to study contact tracing, but their analysis typically depends on a decoupling assumption–most commonly that contact tracing operates on a much faster timescale than disease transmission. Furthermore, contact tracing models often assume that each infected individual becomes a contact tracing-triggering node, which is unrealistic given partial compliance to treatment in practice. In this paper, we relax both of these restrictive assumptions and provide a full analytical characterisation of the epidemic threshold in the pairwise mean-field model. Our analysis uses a fast-variables approach that captures the rapid early stabilisation of key network quantities. In addition, inspired by mechanisms from social adoption dynamics, we introduce triplewise contact tracing in which an infected individual can be traced not only through direct contact with a single tracing-triggering neighbor (pairwise tracing), but also indirectly when connected to two tracing-triggering nodes simultaneously. For pure pairwise and pure triplewise contact tracing, we derive analytical expressions for critical contact tracing thresholds and demonstrate that when

✉ Giulia de Meijere
giulia.demeijere@tuni.fi

✉ István Z. Kiss
istvan.kiss@nulondon.ac.uk

1 Tampere Complexity Lab, Data Science Research Centre, Tampere University, 33720 Tampere, Finland

2 Department of Mathematics, University of Trento, Via Sommarive 14, 38123 Trento, Italy

3 Centro de Ciencias de la Complejidad, Universidad Nacional Autonóma de México, 04510 Ciudad de México, Mexico

4 Institute of Mathematics, Eötvös Loránd University, National Laboratory for Health Security, Budapest, Hungary

5 Network Science Institute, Northeastern University London, London E1W 1LP, UK

6 Department of Mathematics, Northeastern University, Boston MA 02115, USA

Published online: 06 September 2026

many infected individuals bypass treatment, the epidemic can become uncontrollable. When both contact tracing mechanisms operate together, we map out their combined contribution and relative impact on epidemic control. This unified framework yields rigorous and tractable threshold conditions for contact tracing dynamics on networks, extending the applicability of pairwise models beyond the fast-tracing regime and providing new insight into the interplay between disease progression, partial treatment compliance, and higher-order tracing processes.

Mathematics Subject Classification 92D30 · 34C60 · 34C23

1 Introduction

The silent spread of infectious diseases poses a fundamental challenge to epidemic control, particularly when infections exhibit pre-symptomatic transmission, mild symptoms, or asymptomatic progression. Contact tracing—the systematic identification and monitoring of individuals who have been exposed to infected cases—has emerged as a critical non-pharmaceutical intervention that leverages network structure rather than symptomatology to identify at-risk individuals (George et al. 1988). The theoretical foundation for understanding contact tracing efficacy lies at the intersection of network science and mathematical epidemiology, where the explicit consideration of contact patterns becomes essential for accurate predictions (Keeling and Eames 2005).

The mathematical modeling of contact tracing has evolved considerably since the seminal work of Eames et al. (2003), who introduced the Susceptible-Infected-Tracing-Recovered (SITR) framework that explicitly accounts for traced individuals. Their analysis, however, relied on a critical simplifying assumption: that contact tracing operates on a much faster timescale than disease transmission. This assumption, while mathematically convenient, may not hold in practice where tracing delays, limited resources, and imperfect compliance affect the speed and completeness of tracing efforts (Hellewell et al. 2020). Recent empirical evidence from COVID-19 has highlighted that the effectiveness of contact tracing is highly sensitive to delays and adherence rates (Ferretti et al. 2020; Davis et al. 2021), suggesting that relaxing the fast-tracing assumption is crucial for realistic assessment of control strategies.

Network structure fundamentally shapes both disease transmission and the efficacy of contact tracing (Pastor-Satorras et al. 2015). While mean-field models provide analytical tractability, they fail to capture the heterogeneity and clustering present in real contact networks (István Z Kiss et al. 2017). Pairwise approximation models offer a middle ground, incorporating local network structure while maintaining analytical accessibility (Barnard et al. 2019). These models explicitly track pairs of individuals in different states, allowing for the representation of correlations that develop during epidemic spread. The fast-variables approach introduced by Barnard et al. (2019) demonstrated that network quantities such as the average number of susceptible neighbors per infected individual reach quasi-equilibrium rapidly, providing a novel pathway to derive epidemic thresholds without requiring the problematic linearization around disease-free steady-state.

The mechanisms of contact tracing itself have also evolved beyond simple forward tracing. Bidirectional tracing, which identifies both contacts and sources of infection, has been shown to dramatically improve control efficacy (Bradshaw et al. 2021). Similarly, backward tracing—prioritizing the identification of infection sources—can be particularly effective in networks with heterogeneous transmission (Kojaku et al. 2021). These enhanced tracing strategies suggest that the classical pairwise tracing model may be insufficient to capture the full spectrum of tracing mechanisms available to public health authorities. In branching-process and probabilistic epidemic models, the traced set is defined through infection ancestry rather than through local contact relationships, which makes them particularly well suited to this type of investigation (Allan and Brandt 2022; Giulia De Meijere et al. 2023).

Recent theoretical advances have emphasized the importance of higher-order network structures in epidemic dynamics. House et al. (2009) developed a motif-based approach that systematically incorporates triangles and other small subgraphs, demonstrating that clustering and other higher-order structures can significantly alter epidemic thresholds. This motivates the consideration of triplewise interactions in contact tracing, where an individual might be traced through multiple pathways or require multiple exposures to tracing signals before taking action—a mechanism analogous to complex contagion in social networks.

The timing and effectiveness of contact tracing are constrained by fundamental epidemiological parameters (Mettler et al. 2021). Fraser et al. (2004) identified key factors determining outbreak controllability, emphasizing the critical role of the proportion of transmission occurring before symptom onset. For diseases with substantial pre-symptomatic transmission, the window for effective contact tracing narrows considerably, making rapid and comprehensive tracing essential. This underscores the importance of developing models that can accurately capture the interplay between tracing speed, coverage, and disease natural history.

The comprehensive review by Müller and Kretzschmar (2021) highlights the diversity of contact tracing models and their varying predictions about efficacy, emphasizing the need for careful consideration of model assumptions. Network-based approaches have proven particularly valuable, as demonstrated by Miller (2011) and extended in the comprehensive treatment by István Z Kiss et al. (2017). The challenge of selecting appropriate model structures for emerging epidemics has been systematically addressed by Pellis et al. (2015) and Ball et al. (2015), who emphasize the trade-offs between model complexity and analytical tractability.

In this paper, we extend the analytical framework for contact tracing on networks by addressing two key limitations of existing models. First, we relax the assumption of infinitely fast contact tracing, allowing for realistic timescales where tracing and transmission operate concurrently. Second, we introduce a novel triplewise contact tracing mechanism, where individuals require exposure to multiple traced neighbors before taking action. This mechanism captures scenarios where social reinforcement or institutional thresholds govern behavioral responses to tracing notifications. Using the fast-variables approach, we derive explicit threshold conditions for epidemic control under both pairwise and triplewise tracing, providing analytical insights that remain valid across the full parameter space. Our results reveal that contact tracing effectiveness depends critically on network structure, with the required tracing effort scaling

non-linearly with network degree. These findings provide a rigorous foundation for designing contact tracing strategies that account for realistic operational constraints and behavioral responses.

2 Model

We propose an extension of the 'SITR' (Susceptible-Infected-Tracing-Recovered) epidemic model for contact tracing (CT) introduced in Eames et al. (2003). The model of Eames et al. (2003) builds on the standard SIR (Susceptible–Infected–Recovered) epidemic framework (Kermack and McKendrick 1927). New infections occur at rate τ, conditional on contact between a susceptible individual S and an infected, infectious individual I. Infected individuals leave the infectious state at rate g and enter a treated (tracing) state T, in which they are no longer contagious. This state represents, for example, individuals who recover prematurely due to treatment or who adopt interventions that fully prevent onward transmission, such as effective mask use. Importantly, treated individuals may also influence their infected neighbors to seek treatment. This contact tracing mechanism induces additional transitions from I to T at rate c_p, conditional on pairwise interaction between treated and infected individuals. Finally, treated individuals cease tracing activity at rate a and move to the recovered state R, which is absorbing.

We work under the assumption of stable contact patterns between individuals, such as those occurring within households and workplaces. We can then safely assume that when a node becomes tracing-triggering and engages in non-infectious interactions with nodes in I which it traces, it is roughly equivalent to the tracing-triggering node contacting the infected contacts which it interacted with prior to becoming tracing-triggering. Assuming such time invariance, the period of active tracing activity (set through the rate a) is an acceptable approximation of the period over which index cases are asked by health authorities to recall past contacts. Instead, the rate of contact tracing c_p can be interpreted as an effective tracing success rate, incorporating both the identification and recollection of an index case's contacts and their subsequent compliance with recommended protective measures.

In the present work, we propose two extensions of this skeleton model. First, we allow a partial compliance of the infected population to treatment: infected individuals may recover following the natural course of infection, without ever seeking treatment. We call this the natural recovery rate h. Second, we allow for a higher-order version of contact tracing by requiring the exposure of an infected individual in I to two treated individuals in T for a transition to occur from I to T, with new rate c_t. This triplewise form of contact tracing may account for greater reluctance to adopt protective behaviors when traced by infected contacts, so that a single infected individual is more likely to be successfully traced when it is reported by multiple contacts. The triplewise contact tracing may also account for more spontaneous and informal implementations of contact tracing which rely more on social reinforcement driving the spontaneous adoption of protective behaviors. Note that triplewise contact tracing is in general not equivalent to the standard absolute threshold model with threshold $\theta = 2$ (Starnini

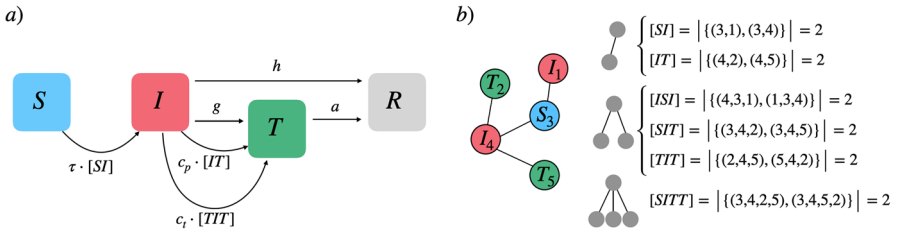


Fig. 1 Schematic description of the epidemic model. **a** Individuals exist in four states: susceptible S, infected I, treated (tracing) T, and recovered R. A susceptible individual becomes infected at rate τ, conditional on an $[SI]$ contact. An infected individual either recovers naturally at rate h or seeks treatment at rate g, thereby moving to the treated state and initiating contact tracing. Treated individuals exit T at rate a and move to R. In addition, infected individuals move to T through contact tracing at rate c_p conditional on an $[IT]$ contact, and at rate c_t conditional on a $[TIT]$ triple. **b** Sample network of 5 nodes (one in state S, two in state I, and two in state T) and 4 edges, and counts of the local network structures that appear in the network: pairs $[AB]$, triples $[ABC]$ and 3-stars $[AEBC]$ (E is the state of the center node of the 3-star). The subscripts of node states denote node identities, and the tuple notation (x, y, z) indicates that node with identity x has an edge with node with identity y who has an edge with node z

Table 1 Summary and domain of the model parameters, when applicable, before and after non-dimensionalisation by the natural timescale $g + h$

Name	Dimensional	Non-dimensional	Domain
Rate of infection	τ	τ	$\mathbb{R}^+$
Rate of recovery of treated individuals	a	a	$\mathbb{R}^+$
Rate of spontaneous adoption of treatment	g	q	$\mathbb{R}^+$
Rate of natural recovery	h	$1 - q$	$\mathbb{R}^+$
Rate of pairwise tracing	c_p	c_p	$\mathbb{R}^+$
Rate of triplewise tracing	c_t	c_t	$\mathbb{R}^+$
Number of nodes in the network	N		$\mathbb{N}$
Average degree of the nodes in the network	n		$\mathbb{N}$
Basic reproductive number		$R_0 : \tau(n-2)$	$\mathbb{R}^+$

et al. 2025). Indeed, in our model, compliance with CT is only possible, not guaranteed, once the threshold has been reached.

A schematic representation of the full compartmental model for CT is provided in Fig. 1a and Table 1 summarizes the model parameters.

To capture correlations arising from contact tracing, we formulate the model within the pairwise approximation framework (István Z Kiss et al. 2017). In addition to tracking the expected number of individuals in each epidemiological state, we explicitly follow the dynamics of connected pairs of individuals. Let $[A]$ denote the expected number of nodes in state $A \in \{S, I, T, R\}$, and $[AB]$ the expected number of edges connecting nodes in states A and B, irrespective of order. The evolution of node- and pair-level quantities is derived by accounting for all events that create or destroy nodes or edges of a given type. As tracing mechanisms depend explicitly on local network structure (Eames et al. 2003), higher-order motifs naturally arise in the description: triples of the form $[ABC]$ represent connected paths of length two, while four-node

motifs $[AEBC]$ correspond to 3-stars centered at node E. The network motifs encode the local configurations required for pairwise and triplewise tracing events (see Fig. 1b) and appear explicitly in the resulting open system of equations, as shown below:

$$\begin{cases} [\dot{S}] &= -\tau[SI] \\ [\dot{I}] &= \tau[SI] - (g+h)[I] - c_p[IT] - c_t[TIT] \\ [\dot{T}] &= g[I] + c_p[IT] - a[T] + c_t[TIT] \\ [\dot{R}] &= a[T] + h[I] \\ [\dot{SS}] &= -2\tau[SSI] \\ [\dot{SI}] &= \tau([SSI] - [ISI] - [SI]) - c_p[SIT] - (g+h)[SI] - c_t[SITT] \\ [\dot{ST}] &= -\tau[IST] + g[SI] + c_p[SIT] - a[ST] + c_t[SITT] \\ [\dot{II}] &= 2\tau([SI] + [ISI]) - 2(g+h)[II] - 2c_p[IIT] - 2c_t[IITT] \\ [\dot{IT}] &= \tau[IST] - a[IT] + c_p([IIT] - [TIT] - [IT]) + g[II] \\ & \quad -(g+h)[IT] + c_t[IITT] - c_t([TIT] + [TITT]) \\ [\dot{TT}] &= 2g[IT] + 2c_p([IT] + [TIT]) + 2c_t([TIT] + [TITT]) - 2a[TT] \end{cases} \tag{2.1}$$

The terms proportional to τ correspond to infection events along $S-I$ edges, as in the standard pairwise SIR model. The terms proportional to g and h describe spontaneous transitions $I \to T$ (self-reporting or background detection) and $I \to R$, respectively, while a governs removal of treated individuals. The terms proportional to c_p capture pairwise contact tracing: these involve motifs such as $[IT]$, $[SIT]$, and $[IIT]$, reflecting tracing triggered by a treated neighbor. The terms proportional to c_t represent triplewise tracing mechanisms and depend on higher-order motifs such as $[TIT]$, $[SITT]$, and $[IITT]$, encoding configurations in which tracing is activated through the presence of not one but two contacts in state T. If a motif contains multiple interchangeable nodes in the same state, permutations of these nodes are equivalent and contribute a symmetry factor. For example, the destruction of an $[SS]$ pair can occur through the infection, with rate τ, of either of the susceptible interchangeable nodes in the triple $[SSI]$. The equations in Eq. (2.1) are written by considering all the possible ways of creating and destroying specific motifs. For instance, the pair $[SI]$ between an infected and a susceptible node can only be created through the infection of a susceptible individual in a $[SSI]$ triple. On the other hand, there exist multiple ways of destroying the $[SI]$ pair: through the infection of the susceptible node of the pair, either by the infected node in the pair or by another infected node, and alternatively, by the pairwise or triplewise tracing of the infected node of the pair.

In Eq. (2.1), the changes in the counts of pairs depend on the counts of triples and four-motifs, whose changes would depend on progressively higher-order motifs. The model thus forms an open hierarchy, which may be closed using standard moment-closure approximations. We consider the following standard closure for the triple (Keeling and Eames 2005):

$$[ABC] = \frac{(n-1)}{n} \frac{[AB][BC]}{[B]}, \tag{2.2}$$

where n is the average degree. For the 4-motif, assuming a star structure and based on House et al. (2009), the closure reads:

$$\begin{aligned}[AEBC] &= [*]\frac{[-]^3}{[<]^3[.]}\frac{[AEB][AEC][BEC]}{[AE][BE][CE]}\cdot[E] \\ &= \frac{(n-1)(n-2)}{n^2}\frac{[AE][BE][CE]}{[E]^2},\end{aligned} \tag{2.3}$$

where the number of nodes is $[\cdot] = N$, the number of pairs is $[-] = nN$, the number of triples is $[<] = Nn(n-1)$, and the number of 3-stars is $[*] = Nn(n-1)(n-2)$.

Using these closures, the dynamics becomes:

$$\begin{cases}
[\dot{S}] &= -\tau[SI] \\
[\dot{I}] &= \tau[SI] - [I] - c_p[IT] - c_t\frac{n-1}{n}\frac{[IT]^2}{[I]} \\
[\dot{T}] &= q[I] + c_p[IT] - a[T] + c_t\frac{n-1}{n}\frac{[IT]^2}{[I]} \\
[\dot{R}] &= a[T] + (1-q)[I] \\
[\dot{SS}] &= -2\tau\frac{n-1}{n}\frac{[SS][SI]}{[S]} \\
[\dot{SI}] &= \tau(\frac{n-1}{n}\frac{[SS][SI]}{[S]} - \frac{n-1}{n}\frac{[SI]^2}{[S]} - [SI]) - c_p\frac{n-1}{n}\frac{[SI][IT]}{[I]} - [SI] - c_t\frac{(n-1)(n-2)}{n^2}\frac{[SI][IT]^2}{[I]^2} \\
[\dot{ST}] &= -\tau\frac{n-1}{n}\frac{[SI][ST]}{[S]} + q[SI] + c_p\frac{n-1}{n}\frac{[SI][IT]}{[I]} - a[ST] + c_t\frac{(n-1)(n-2)}{n^2}\frac{[SI][IT]^2}{[I]^2} \\
[\dot{II}] &= 2\tau([SI] + \frac{n-1}{n}\frac{[SI]^2}{[S]}) - 2[II] - 2c_p\frac{n-1}{n}\frac{[II][IT]}{[I]} - 2c_t\frac{(n-1)(n-2)}{n^2}\frac{[II][IT]^2}{[I]^2} \\
[\dot{IT}] &= \tau\frac{n-1}{n}\frac{[SI][ST]}{[S]} - a[IT] + c_p(\frac{n-1}{n}\frac{[II][IT]}{[I]} - \frac{n-1}{n}\frac{[IT]^2}{[I]} - [IT]) + q[II] - [IT] \\
&\quad + c_t\frac{(n-1)(n-2)}{n^2}\frac{[II][IT]^2}{[I]^2} - c_t(\frac{n-1}{n}\frac{[IT]^2}{[I]} + \frac{(n-1)(n-2)}{n^2}\frac{[IT]^3}{[I]^2}) \\
[\dot{TT}] &= 2q[IT] + 2c_p([IT] + \frac{n-1}{n}\frac{[IT]^2}{[I]}) + 2c_t(\frac{n-1}{n}\frac{[IT]^2}{[I]} + \frac{(n-1)(n-2)}{n^2}\frac{[IT]^3}{[I]^2}) - 2a[TT]
\end{cases} \tag{2.4}$$

where the transition rates have been renormalized by the natural timescale $g + h$:

$$\tau \leftarrow \frac{\tau}{g+h},\ c_p \leftarrow \frac{c_p}{g+h},\ c_t \leftarrow \frac{c_t}{g+h},\ a \leftarrow \frac{a}{g+h},\ \text{and } q := \frac{g}{g+h}.$$

From here onward, we only consider the time-scaled transition rates.

When $q = 0$, natural recovery dominates over the transition to the treated state, yielding the classical SIR model. Similarly, when $a \to \infty$, individuals reside in the treated state for a vanishing duration, and we recover the SIR model. Instead, when $q \to 1$ (no bypass of the treated state T) and $c_t = 0$ (no triplewise contact tracing), we recover the original model by Eames et al. (2003).

The usual way of calculating threshold values of parameters is to evaluate the leading eigenvalue of the Jacobian of the system at the disease-free steady-state. For the pairwise SITR model [Eq. (2.4)], this approach is not directly applicable, since the closure relations become ill-defined at the disease-free steady-state due to the presence of $[I] = 0$ in the denominator. Nevertheless, the threshold can be identified numerically, as demonstrated in Appendix C. Moreover, in what follows, we present a mathematical method based on fast variables that is able to capture the threshold behaviour analytically, yielding threshold values that agree well with the numerical results.

3 Results

In this section, we show that although incorporating a local network structure renders standard linear stability analysis unable to determine the critical contact tracing threshold, this limitation can be overcome by exploiting correlations emerging at early times.

Indeed, we first show that early-time correlations govern a reformulation of the epidemic threshold problem in terms of so-called 'fast variables'. This alternative approach reveals that the contact tracing benefits from a network structure when it comes to its contribution to outbreak eradication. We then show analytically how the success of contact tracing heavily depends on the density of the network structure, the contact tracing coverage level, and its timescale relative to disease progression.

3.1 Epidemic threshold via fast variables

In linear stability analysis, the epidemic threshold is defined by the critical parameter values at which the disease-free steady state loses stability. Equivalently, this threshold corresponds to the point in parameter space where the growth rate of the infected population vanishes. The condition of zero growth therefore provides a necessary and sufficient criterion for the epidemic threshold. In the equation for the growth of the number of infected individuals $[\dot{I}]$ in Eq. (2.4), $[I]$ can be factorized to give:

$$\frac{[\dot{I}]}{[I]} = \tau \frac{[SI]}{[I]} - 1 - c_p \frac{[IT]}{[I]} - c_t \frac{n-1}{n} \left(\frac{[IT]}{[I]} \right)^2, \tag{3.1}$$

and the vanishing of the right hand side separates regimes of exponential growth and decay of the number of infected individuals. Based on this reformulation, the epidemic threshold depends on the limiting values of $[SI]/[I]$ and $[IT]/[I]$.

Motivated by this observation, we define the new variables $x(t) := [SI]/[I]$ and $z(t) := [IT]/[I]$. To find their limiting values, we set down the equations for their time evolution $\dot{x} = [\dot{SI}]/[I] - x[\dot{I}]/[I]$ and $\dot{z} = [\dot{IT}]/[I] - z[\dot{I}]/[I]$. Writing the equations for $[\dot{SI}]/[I]$, $[\dot{IT}]/[I]$, and $[\dot{I}]/[I]$ using Eq. (2.4) eventually requires to define and find the limiting values of the following set of new variables (see Appendix A):

$$\begin{aligned} x(t) &= \frac{[SI]}{[I]}, \quad z(t) = \frac{[IT]}{[I]}, \quad \text{and} \quad y(t) := \frac{[II]}{[I]}, \quad u(t) := \frac{[SS]}{[S]}, \\ v(t) &:= \frac{[SI]}{[S]}, \quad w(t) := \frac{[ST]}{[S]}. \end{aligned} \tag{3.2}$$

Barnard et al. show in Barnard et al. (2019) that, as illustrated in Fig. 2, these so-called 'fast' variables reach a transient equilibrium much faster compared to the time scale of epidemic evolution. Indeed, early on in an epidemic a correlation structure is formed that drives this early saturation of variables. 'Waiting' for the epidemic to 'feel' the network turns out to be the only reasonable way to measure the epidemic threshold.

Overall, the epidemic threshold can be obtained by identifying the conditions on the model parameters that cancel the growth of the prevalence $[\dot{I}]$ once the fast variables have reached their steady state. We thus need to solve:

$$\dot{x} = 0, \quad \dot{z} = 0, \quad \dot{y} = 0, \quad \dot{u} = 0, \quad \dot{v} = 0, \quad \dot{w} = 0, \quad \text{and} \quad \frac{[\dot{I}]}{[I]} = 0. \tag{3.3}$$

Proximity with the initial condition. Assuming proximity with the initial condition, we can impose u constant and equal to the average degree n, which holds as long as the initial epidemic seed is small and mixes randomly with the susceptible population: $[SS](0) \sim nN$ and $[S](0) \sim N$. Initially, we can also assume that both v and w are constant and equal to zero, since $[SI](0) \sim [ST](0) \sim 0$.

This approximation reduces Eq. (3.3) to:

$$\dot{x} = 0, \quad \dot{y} = 0, \quad \dot{z} = 0, \quad \frac{[\dot{I}]}{[I]} = 0, \tag{3.4}$$

where, using Eq. (2.4), we have

$$\begin{cases} \dot{x} &= \frac{[\dot{S}I]}{[I]} - x\frac{[\dot{I}]}{[I]} \\ &= \tau x(n-2) + \frac{c_p}{n}xz + 2\frac{c_t}{n}\frac{n-1}{n}xz^2 - \tau x^2, \\ \dot{y} &= \frac{[\dot{I}I]}{[I]} - y\frac{[\dot{I}]}{[I]} \\ &= \tau x(2-y) - y - \frac{n-2}{n}c_p yz - \frac{n-1}{n}\frac{n-4}{n}c_t yz^2, \\ \dot{z} &= \frac{[\dot{I}T]}{[I]} - z\frac{[\dot{I}]}{[I]} \\ &= -\tau xz - (a+c_p)z + c_p\frac{n-1}{n}yz + \frac{c_p}{n}z^2 + qy + c_t\frac{(n-1)(n-2)}{n^2}yz^2 - c_t\frac{n-1}{n}z^2 + c_t\frac{2}{n}\frac{n-1}{n}z^3. \end{cases} \tag{3.5}$$

Eventually, the epidemic threshold can be computed from Eq. (3.4) or equivalently from:

$$\frac{[\dot{I}]}{[I]} = 0, \quad \frac{[\dot{S}I]}{[I]} = 0, \quad \frac{[\dot{I}I]}{[I]} = 0, \quad \frac{[\dot{I}T]}{[I]} = 0. \tag{3.6}$$

Using the definition of the fast variables [Eq. (3.2)] and dividing the equations for $[\dot{S}I]$, $[\dot{I}I]$, and $[\dot{I}T]$ in Eq. (2.4) by $[I]$, Eq. (3.6) finally reads:

$$\begin{cases} \tau x - 1 - c_p z - c_t\frac{(n-1)}{n}z^2 = 0 \\ \tau x(n-2) - c_p\frac{(n-1)}{n}xz - x - c_t\frac{(n-1)(n-2)}{n^2}xz^2 = 0 \\ 2\tau x - 2y - 2c_p\frac{(n-1)}{n}yz - 2c_t\frac{(n-1)(n-2)}{n^2}yz^2 = 0 \\ -az + c_p\left(\frac{(n-1)}{n}yz - \frac{(n-1)}{n}z^2 - z\right) + (qy - z) \\ \qquad + c_t\frac{(n-1)(n-2)}{n^2}yz^2 - c_t\frac{(n-1)}{n}z^2 - c_t\frac{(n-1)(n-2)}{n^2}z^3 = 0. \end{cases} \tag{3.7}$$

Here, contact tracing, through its parameters c_p and c_t, influences the derivation of the epidemic threshold, in contrast to the homogeneous mean-field formulation of the model, where it has no effect (see Appendix B). We can thus compute the level of contact tracing (c_p or c_t) that is required to bring the system to the disease-free

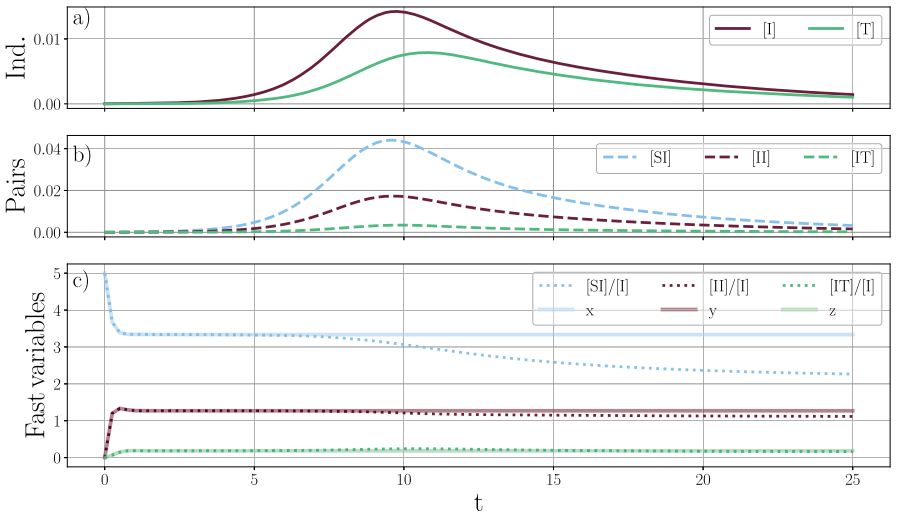


Fig. 2 The fast variables reach a transient equilibrium much sooner compared to the time scale of epidemic evolution. **a** Time evolution of $[I]$ and $[T]$. **b** Time evolution of the pairs $[SI]$, $[II]$, and $[IT]$. c) Time evolution of the fast variables x, y, and z, computed from the full system in Eq. (2.4) (dotted line) or from the fast-variables system in Eq. (3.5) (solid line). Parameter values: $n = 5$, $\tau = 1.1$, $a = 1$, $q = 0.6$, $c_p = 10$, and $c_t = 0$ (pure pairwise). Initial conditions: $[I](t = 0) = [T](t = 0) = 10^{-5}$

steady-state. In Appendix C, we show through numeric solving of the ODE system in Eq. (2.4) that the critical level of contact tracing computed in this way separates a regime where the number of infected individuals in the population grows or decays exponentially fast, once the fast variables have reached a transient steady-state. There, we also show that the critical level of tracing also separates regimes where a zero or nonzero final epidemic size (stationary number of recovered individuals) can be reached with an infinitesimal infected seed.

3.2 Critical thresholds for control

Leveraging early time correlations with the help of fast variables, we were able to reformulate the epidemic threshold problem in terms of growth and decay of the population of infected individuals. We found that, when accounting for a local network structure through a pairwise representation, the contact tracing parameters affect the capacity of the system to reach the disease-free steady-state and thus, we can look for a critical level of contact tracing.

In this section, we first analyze the pure pairwise and pure triplewise scenarios separately. We then discuss the differences between the two distinct implementations of contact tracing and the consequences of combining them.

3.2.1 Pairwise contact tracing

First, we consider that an individual in state T can independently influence each of its infected neighbors in I into seeking treatment. This mechanism of pairwise

social influence corresponds for example to the digital and manual implementations of contact tracing in an airborne disease outbreak, whereby confirmed cases who wear face masks inform their contacts about their infected status, eventually influencing them into considering adoption of mitigation measures too.

The critical level of contact tracing can be derived from Eq. (3.7) (more details in Appendix D), by identifying the pure pairwise contact tracing parameter c_p that solves the system, under the constraint of no triplewise contact tracing, i.e. $c_t = 0$. In this case, the critical level of pairwise contact tracing required to eradicate the spreading disease is:

$$c_p^* = (a + R_0)\,\frac{R_0 - 1}{F_p(n, q, \tau)}, \tag{3.8}$$

where $F_p(n, q, \tau) := \frac{1}{n}\frac{R_0(nq-1)+(1-q)}{R_0}$, and $R_0 := \tau(n-2)$ is the basic reproductive number (note that τ is the ratio between the infection rate and the total recovery rate, and that the factor $(n-2)$ accounts for pairwise correlation structures (Eames et al. 2003; Keeling 1999)).

When the compliance gets large $q \to 1$, F_p satisfies $F_p(n, 1, \tau) = \frac{n-1}{n}$, which is the pre-factor of the closure of triples. Instead, a lower bound $q^p_{\min} \leq q$ on the compliance with treatment or tracing coverage is imposed by the condition $c_p^* \geq 0$, with $q^p_{\min} = \frac{R_0-1}{R_0 n-1}$. When the coverage approaches its lower bound $q \to (q^p_{\min})^+$, $F_p \to 0$ and the critical level of contact tracing $c_p^* \to \infty$ diverges. Thus, when tracing coverage becomes too small $q < q^p_{\min}$, no finite level of pairwise CT is able to contain an epidemic. In Fig. 3a, we see for several values of the spreading rate τ, how the critical level of pairwise tracing diverges when $q \to (q^p_{\min})^+$ and then decays with $q > q^p_{\min}$. Although the tracing coverage is expected to affect the performance of contact tracing, we here show that a minimum coverage needs to be reached for contact tracing to be able to contribute to suppressing an outbreak. Moreover, the impact of the tracing coverage is such that a change of 20% in its magnitude can require a 10 times higher level of contact tracing.

We stress that the critical level of contact tracing in Eq. (3.8) is obtained without working under the unrealistic fast tracing assumption used in the seminal work of Eames and Keeling on contact tracing (Eames et al. 2003). For a direct comparison with the result of Eames and Keeling in Eames et al. (2003), we recall that their model considers $q = 1$, so also $F_p = \frac{n-1}{n}$. In addition, fast contact tracing is imposed by scaling the contact rates c_p and a as Λc_p and Λa, with $\Lambda \gg 1$, while leaving all other rates (disease progression rates) unchanged. While the threshold of Eames and Keeling reads

$$(c_p^*)^{\mathrm{EK}} = a\frac{(R_0 - 1)n}{n - 1}, \tag{3.9}$$

we find that the critical level of pairwise contact tracing is generally larger:

$$c_p^* = a\left(1 + \frac{R_0}{\Lambda a}\right)\frac{(R_0 - 1)n}{n - 1} \tag{3.10}$$

$$= \left(1 + \frac{R_0}{\Lambda a}\right)(c_p^*)^{\mathrm{EK}}. \tag{3.11}$$

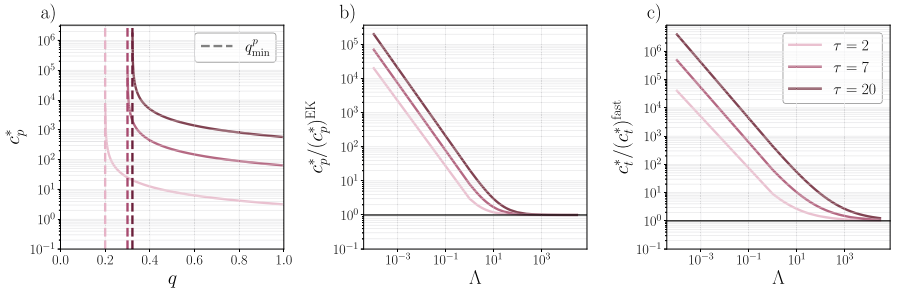


Fig. 3 The threshold diverges for low tracing coverage and slow CT. **a** Critical level of pairwise CT as a function of the tracing coverage q, for three values of the transmission rate: $\tau = 2, 7, 20$. The dashed vertical lines represent $q^p_{\min}$. Parameter value: $a = 0.1$. **b** Ratio between the pure pairwise critical level of CT computed with the method of fast variables (c^*_p) and the Eames and Keeling (EK) threshold ($(c^*_p)^{EK}$), as a function of the celerity of CT, through Λ. We consider the same three values of transmission rate as in panel a, and $c_t = 0$. **c**) Ratio between the pure triplewise critical level of CT computed with the method of fast variables (c^*_t) and the pure triplewise critical level obtained in the adjusted fast tracing limit ($(c^*_t)^{fast}$), as a function of the celerity of CT, through Λ. We consider the same three values of transmission rate as in panel a, and $c_p = 0$. Parameter values for panels b and c: $q = 1$, and $a = 1$. Parameter values common across the three panels: $n = 3$

In Fig. 3b, we show how the fast variables threshold of Eq. (3.8) compares with the Eames and Keeling threshold of Eq. (3.9), when $q = 1$ and for different values of Λ. When CT is slow compared to the disease progression and $\Lambda \ll 1$, we see that the actual level of tracing required to eradicate a disease can be orders of magnitude higher than what expected under the fast tracing assumption. As expected, the agreement improves when Λ grows. In the fast tracing limit, the critical level of tracing depends linearly on the basic reproductive number and is affected by the density (through n) and the period of active tracing (through a). When contact tracing becomes progressively slower, the quadratic dependence on the basic reproductive number becomes important, eventually taking over, and the dependence on a disappears. Overall, Fig. 3a and 3b shows that low tracing coverage and slow contact tracing compared to the timescale of disease progression can significantly undermine the efficacy of the contact tracing measure in bringing the system to the disease-free steady-state. Taken together, these findings mean that contact tracing breaks down, when the basic reproductive number grows too high (relative to the speed of contact tracing).

In Fig. 4, we show that also the network density significantly affects the containment capacity of contact tracing, especially away from the fast contact tracing limit. Similarly to Eames et al. (2003), we let $\tau/(\tau + 1)$ be the probability that infection passes across a contact and $(c^*_p/a)/((c^*_p/a)+1)$ the proportion of contacts that need to be traced, i.e., the social weight of the CT measure. In the fast tracing limit, the social weight is independent of the period of tracing activity (through a). However, stepping out of the fast tracing limit by decreasing Λ reveals a dependence of the social weight on a, that reshapes the social weight landscape in the space of parameters. Crucially, the dependence of the social weight on the network density is amplified when contact tracing gets slower.

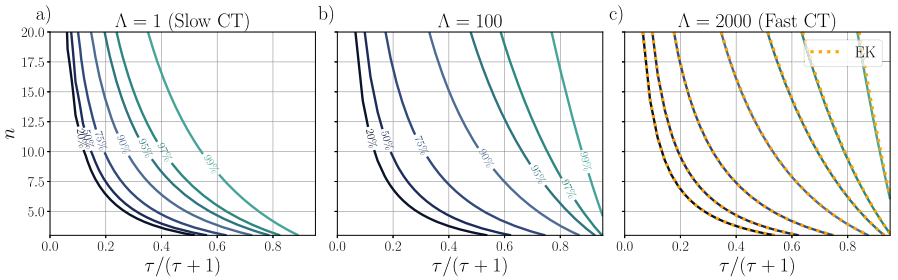


Fig. 4 The social weight of CT increases dramatically for dense networks, as we move away from the fast tracing limit. Contour lines of the (analytical) social weight $(c_p^*/a)/((c_p^*/a)+1)$ in the following plane: network density n vs probability that infection passes across a contact $\tau/(\tau+1)$. a) Fast variables result when $\Lambda = 1$. b) Fast variables result when $\Lambda = 100$. c) Eames and Keeling's (EK) fast tracing result (dashed black lines) superimposed on the fast variables result when $\Lambda = 2000$. Parameter values: $c_t = 0$, $a = 1$, and $q = 1$

3.2.2 Triplewise contact tracing

Formal implementations of contact tracing through digital applications or healthcare manual efforts often require a single pairwise interaction to trigger a contact tracing notification and to encourage the traced individual to seek treatment. In this sense, formal implementations of contact tracing are relatively well captured by the pairwise implementation described in the previous section (Barrat et al. 2021).

Nevertheless, beyond such formal implementations, contact tracing can also arise informally when awareness of an outbreak spreads within a population. In informal settings, individuals influence one another to exchange information about potential exposures and to adopt protective behaviors, generating tracing-like effects through social interactions. This spontaneous, decentralized contact tracing closely resembles opinion-dynamics–driven behavioral adoption (Peralta et al. 2025; Starnini et al. 2025) and may require social reinforcement through exposure to multiple contacts. In this section, we study the pure triplewise implementation of contact tracing, where individuals only get traced if they have been in contact with at least two contact tracing-triggering nodes. This implementation of contact tracing may also describe the adoption of contact tracing by individuals who are particularly reluctant to engage with the process.

Solving Eq. (3.7) (details in Appendix E) for c_t with $c_p = 0$ (no pairwise contact tracing), we find that the critical level of triplewise contact tracing required to eradicate the spreading infection is:

$$c_t^* = (a + R_0)^2 \frac{R_0 - 1}{F_t(n, q, \tau)}, \tag{3.12}$$

where $F_t(n, q, \tau) = \frac{(n-1)}{n^2(n-2)} \left(\frac{R_0(nq-2)+2(1-q)}{R_0} \right)^2$.

When the tracing coverage becomes large $q \to 1$, F_t satisfies $F_t(n, 1, \tau) = \frac{(n-1)(n-2)}{n^2}$, which is the pre-factor of the closure of 3-stars. Moreover, we have a lower bound on the compliance with treatment: $q \geq q_{\min}^t = 2\frac{R_0-1}{R_0 n-2}$, and when the

tracing coverage approaches its lower bound $q \to (q^t_{\min})^+$, $F_t \to 0$ and the critical level of CT $c^*_t \to \infty$ diverges.

The critical level of triplewise tracing exhibits a similar structure to the one of pairwise tracing, with a dependence on tracing coverage, network density, and speed of contact tracing. However, in this case, if we define the fast tracing limit in an analogous way to Eames and Keeling (scaling both the contact tracing rates c_p and a as Λc_p and Λa, with $\Lambda \gg 1$) would make the critical level of triplewise contact tracing diverge. Indeed, when contact tracing is too fast, contact-tracing-triggering nodes terminate their tracing activity so fast that $[TIT]$ triples become too rare and contact tracing fails. However, we can define an alternative and more meaningful fast tracing limit for this form of contact tracing by scaling a as $\sqrt{\Lambda}a$, where $\Lambda \gg 1$ is the scaling of $c_t \to c_t \Lambda$. This fast tracing limit adjusted to the features of triplewise contact tracing is characterized by an enhanced longevity of active tracing. While the critical level of triplewise contact tracing in the adjusted fast tracing limit (assuming no bypass of treatment, $q = 1$) reads:

$$(c^*_t)^{fast} = a^2 n^2 \frac{R_0 - 1}{(n-1)(n-2)}, \tag{3.13}$$

in general it may be significantly larger:

$$c^*_t = \left(1 + \frac{R_0}{\sqrt{\Lambda}a}\right)^2 (c^*_t)^{fast}. \tag{3.14}$$

In Fig. 3c, we show that in the adjusted fast tracing limit, as long as CT is sufficiently fast, the R_0 term may be neglected next to a in Eq. (3.12), similarly to what we observed for pure pairwise CT (panel b).

3.2.3 Epidemic control under combined tracing interventions

Naturally, during an outbreak, the formal and informal implementations of contact tracing can coexist. In this section, we compare the efficacy of the pure pairwise and triplewise implementations of contact tracing before investigating the consequence of combining them.

In Fig. 5a we show, for a representative choice of the parameters, that pure triplewise contact tracing always requires higher rates of contact tracing than pure pairwise, to bring the system to the disease free equilibrium. Additionally, pure triplewise CT systematically needs higher tracing coverages in order to be efficient. Although the critical level of CT grows for denser networks, network density helps expand the range of coverages that are sufficient for the contact tracing measure to be efficient.

Finally, the combination of both types of contact tracing only results in a slight reinforcement of contact tracing, which can be attributed to the correlations between pairwise and triplewise contact tracing. In Fig. 5b, we show how the final epidemic size varies for different combinations of the contact tracing rates c_p and c_t. As mentioned above, the critical rates of contact tracing coincide with the rates that separate a vanishing from a non-vanishing final epidemic size. If both types of contact tracing

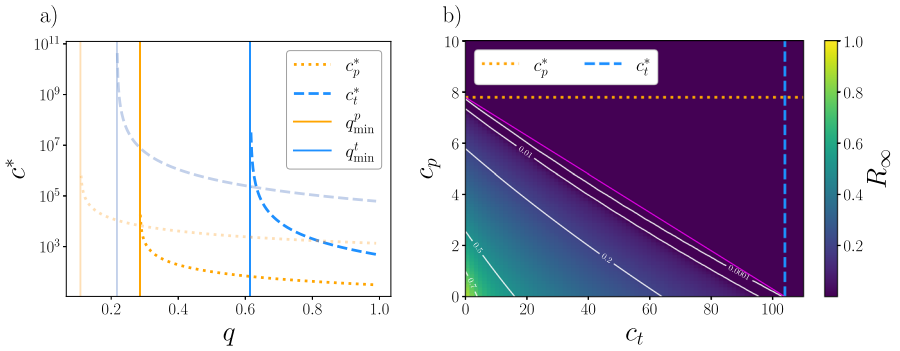


Fig. 5 Triplewise CT is more stringent and less efficient than pairwise CT. **a** Analytical critical level of CT as a function of the tracing coverage q for both pairwise (dotted, orange) and triplewise (dashed, blue) contact tracing. The vertical solid lines indicate the minimum compliance $q_{\min}$. Parameter values: $\tau = 5$, $a = 0.1$, and two choices of the network density, $n = 3$ (full opacity) and $n = 9$ (partial transparency). **b** Heatmap and contour lines of the final epidemic size R_∞ in the following plane: c_p vs c_t. The dotted orange and dashed blue lines are the analytical critical levels of contact tracing for pure pairwise and pure triplewise CT, respectively. Parameter values: $n = 5$, $\tau = 0.7$, $a = 1$, $q = 0.6$. Initial conditions: $[I](0) = [T](0) = 5 \cdot 10^{-8}$

were independent, we would expect the critical levels of contact tracing c_p and c_t to lie on the line connecting the threshold of pure pairwise and pure triplewise contact tracing (solid, magenta line). Instead, we find that when the contact tracing rates of each type –c_p and c_t– are intermediate, the final epidemic size is smaller than would be expected.

4 Conclusion

In a seminal study by Eames and Keeling for pairwise contact tracing on networks (Eames et al. 2003), an analytical expression was derived for the critical level of contact tracing required to suppress an outbreak, under the strong assumption that contact tracing occurs on a timescale much faster than disease progression. This assumption may be reasonable for sexually transmitted infections (STI), for which most major contact tracing programs until the COVID-19 pandemic were deployed (Allan and Brandt 2022; Hossain et al. 2022). Indeed, STIs tend to be associated with long infectious periods (Stephenson 2000), compared to typical times of deployment of contact tracing efforts. However, the assumption of fast contact tracing fails for infectious diseases in general and for airborne infections like COVID-19, in particular.

In this paper, we crucially showed that, by exploiting correlations that arise at early times through the method of fast variables introduced in Barnard et al. (2019), we could overcome both the limitations of standard linear stability analysis in pairwise models and the difficulty of determining critical tracing levels in the general case, when the fast-tracing assumption no longer holds. To do so, we analyzed the ability of contact tracing to drive an epidemic system toward the disease-free state in a pairwise framework. The

pairwise approximation allows us to consider some level of (local) network structure, which is crucial to study an intervention that leverages contact patterns, while keeping the model analytically tractable. Within this setting, we examined two implementations of the intervention: one based on pairwise interactions and another involving triplewise interactions with contact-tracing–triggering nodes. These correspond, respectively, to formal and informal implementations, or to less and more reluctant adoptions of forward contact tracing. To account for evidence on the impact of contact tracing app coverage on the efficacy of the measure, we also considered that only part of the infected populations has the ability to become contact-tracing triggering nodes (Barrat et al. 2021; Moreno López et al. 2021; Mancastroppa et al. 2021).

Additionally, our results show that network density non-linearly influences the effectiveness of contact tracing. While both pairwise and triplewise contact tracing become less efficient as networks become denser (they require a higher critical rate of contact tracing), sufficiently sparse networks are also unfavorable, as they increase the minimum tracing coverage required for contact tracing to be effective, thereby narrowing the range of coverages over which it can contribute. Moreover, by deriving results in full generality, rather than restricting attention to the limit in which contact tracing is much faster than disease progression, we could demonstrate that assuming fast contact tracing can substantially underestimate the required tracing effort and overestimate the efficacy of the intervention. The intervention should be deployed at a pace that is at least comparable to the spreading rate of the disease. Finally, although triplewise contact tracing—representing a more spontaneous or informal implementation of the measure—is always less efficient than its pairwise counterpart, it can still make a meaningful contribution, especially when the spread of protective behaviors through contact tracing occurs on a timescale comparable to that of disease progression or as long as the tracing activity of treated individuals lasts sufficiently long.

To maintain analytical tractability, we deliberately restricted the number of epidemic states, omitting compartments that are often important for more realistic representations of disease progression, such as an exposed state for influenza-like illnesses (Chowell et al. 2008; Trentini et al. 2022). The assumption that contact tracing triggering nodes are no longer infectious is also a strong simplification.

In practice, the tracing of contacts can occur manually and digitally. The former channel for the tracing of contacts operates at large scale but relies on potentially inaccurate contact recollections and costly one-by-one interviews, the latter is accurate and inexpensive but is compromised by partial voluntary app adoption (Mancastroppa et al. 2021; Zhang and Britton 2024). Although beyond the scope of this study, these distinctions affect the pairs of tracing-triggering nodes and infected nodes through which successful tracing may occur. Additionally, our model is designed for the tracing of infected contacts, regardless of their position in the transmission chain. In contrast, distinction between forward, sideward and backward contact tracing can be efficiently studied analytically through a different modelling architecture capable of explicitly tracking infection ancestry: branching process models (de Meijere and Castellano 2023). Despite the power of these models for epidemic modelling (Britton et al. 2016), they are less naturally equipped to capture tracing of infected contacts that do not belong to the same transmission chain, as well

as correlation and saturation effects that develop away from the epidemic's initial phase. Moreover, despite incorporating some level of network representation, we also neglected numerous features of real contact networks such as clustering (House and Keeling 2010), higher-order interactions, and distinct network layers for contact tracing and disease progression (Mancastroppa et al. 2021). Finally, while our analysis focuses on how contact tracing shifts the epidemic threshold, this intervention can also shape the epidemic curve by affecting peak height and timing. These effects are crucial for determining whether the health-care system becomes saturated and for buying time to deploy resources such as diagnostic tests, face masks, and vaccination campaigns to further mitigate the outbreak (Di Domenico et al. 2020).

A natural continuation of this work would account for higher-order contact tracing implementations and study how increasingly high numbers of required tracing notifications for the adoption of protective measures by an infected person would suppress the efficacy of the measure. Although we do not technically assume the absence of changes in contact patterns in the network over time, our representation of contact tracing better matches real implementations of contact tracing if we assume static contact patterns or if we focus on highly recurrent contacts in social foci such as households and workplaces (Ureña-Carrion et al. 2026). Indeed, unlike traditional contact tracing, which identifies contacts made before becoming tracing-triggering (e.g., when a diagnostic test results positive), our model assumes that nodes notify contacts made during a period after becoming tracing-triggering. Under the assumption of static or stable contacts, the two groups of traced neighbors coincide. However, in general networks are highly temporal, undergo turnover and periods of tie latency, and also contain sporadic short lasting interactions (Holme and Saramäki 2012; Newman 2018; Kivelä et al. 2014; Unicomb et al. 2021). In future work, the consequences of this temporal dimension on contact tracing should be taken into account.

Acknowledgements We gratefully acknowledge Prof. Matt Keeling for providing excerpts from Dr Ken Eames' PhD thesis, which enabled us to gain a deeper understanding of the assumptions and results underlying (Eames et al. 2003).

Funding Open access funding provided by Tampere University (including Tampere University Hospital). P.L. Simon acknowledges support from the National Research, Development and Innovation Office in Hungary (RRF−2.3.1-21-2022-00006). G. de Meijere acknowledges support from a Magnus Ehrnroothin säätiö postdoctoral fellowship.

Declarations

Conflict of interest We declare that we have no conflict of interest.

Open Access This article is licensed under a Creative Commons Attribution 4.0 International License, which permits use, sharing, adaptation, distribution and reproduction in any medium or format, as long as you give appropriate credit to the original author(s) and the source, provide a link to the Creative Commons licence, and indicate if changes were made. The images or other third party material in this article are included in the article's Creative Commons licence, unless indicated otherwise in a credit line to the material. If material is not included in the article's Creative Commons licence and your intended use is not permitted

by statutory regulation or exceeds the permitted use, you will need to obtain permission directly from the copyright holder. To view a copy of this licence, visit http://creativecommons.org/licenses/by/4.0/.

A Full system of fast variables

In general, the evolution of x and z is governed by:

$$\begin{cases} \dot{x} &= \frac{[\dot{SI}]}{[I]} - x\frac{[\dot{I}]}{[I]} \\ &= \tau x(\frac{n-1}{n}(u-v)-1) + \frac{c_p}{n}xz + 2\frac{c_t}{n}\frac{n-1}{n}xz^2 - \tau x^2, \\ \dot{z} &= \frac{[\dot{IT}]}{[I]} - z\frac{[\dot{I}]}{[I]} \\ &= \tau x(\frac{n-1}{n}w - z) - (a+c_p)z + c_p\frac{n-1}{n}yz + \frac{c_p}{n}z^2 + qy \\ &\quad + c_t\frac{(n-1)(n-2)}{n^2}yz^2 - c_t\frac{n-1}{n}z^2 + c_t\frac{2}{n}\frac{n-1}{n}z^3, \end{cases} \tag{A.1}$$

where $u := \frac{[SS]}{[S]}$, $v := \frac{[SI]}{[S]}$, $w := \frac{[ST]}{[S]}$, and $y := \frac{[II]}{[I]}$.

We thus also need to write down the evolution of these variables, which reads:

$$\begin{cases} \dot{u} &= \frac{[\dot{SS}]}{[S]} - u\frac{[\dot{S}]}{[S]} \\ &= -\tau(2\frac{n-1}{n}+1)uv, \\ \dot{v} &= \frac{[\dot{SI}]}{[S]} - v\frac{[\dot{S}]}{[S]} \\ &= \tau\frac{n-1}{n}uv + \frac{\tau}{n}v^2 - (\tau-1)v - c_p\frac{n-1}{n}vz - c_t\frac{(n-1)(n-2)}{n^2}vz^2, \\ \dot{w} &= \frac{[\dot{ST}]}{[S]} - w\frac{[\dot{S}]}{[S]} \\ &= \frac{\tau}{n}vw + qv - aw + c_p\frac{n-1}{n}vz + c_t\frac{(n-1)(n-2)}{n^2}vz^2, \\ \dot{y} &= \frac{[\dot{II}]}{[I]} - y\frac{[\dot{I}]}{[I]} \\ &= \tau x(2(1+\frac{n-1}{n}v)-y) - y - \frac{n-2}{n}c_pyz - \frac{n-1}{n}\frac{n-4}{n}c_tyz^2. \end{cases} \tag{A.2}$$

Assuming proximity with the initial condition implies considering u, v, and w as constant and more specifically $u = n$ and $v = w = 0$. This assumption yields the following system of equations for the evolution of fast variables:

$$\begin{cases} \dot{x} = \tau x(\frac{n-1}{n}(n-0)-1) + \frac{c_p}{n}xz + 2\frac{c_t}{n}\frac{n-1}{n}xz^2 \\ \dot{z} = \tau x(0-z) - (a+c_p)z + c_p\frac{n-1}{n}yz + \frac{c_p}{n}z^2 - qz \\ +c_t\frac{(n-1)(n-2)}{n^2}yz^2 - c_t\frac{n-1}{n}z^2 + c_t\frac{2}{n}\frac{n-1}{n}z^3 \\ \dot{u} = 0 \\ \dot{v} = 0 \\ \dot{w} = 0 \\ \dot{y} = \tau x(2(1+0)-y) - y - \frac{n-2}{n}c_pyz - \frac{n-1}{n}\frac{n-4}{n}c_tyz^2. \end{cases} \tag{A.3}$$

An SIS version of this model would only require the addition of a $+az$ term in the $[\dot{SI}]/[I]$ equation.

B Homogeneous mean-field approximation

Under the homogeneous mean-field approximation, we can write the ordinary differential equations (ODE) describing the time evolution of the number of nodes in each state:

$$\begin{cases} \dot{S} &= -\tau I S \\ \dot{I} &= +\tau I S - (g+h) I - c_p T I - c_t I T^2 \\ \dot{T} &= g I + c_p T I - a T + c_t I T^2 \\ \dot{R} &= a T + h I. \end{cases} \tag{B.1}$$

Identifying the epidemic threshold in this context corresponds to finding the condition on the model parameters that makes the leading eigenvalue of the Jacobian at the disease-free steady-state equal to zero. This condition separates a regime where the disease-free steady-state is locally stable from one where it is not. Linearizing Eq. (B.1) around the disease-free state immediately eliminates all contributions of contact tracing (through its parameters c_p and c_t) to the epidemic threshold, thereby suggesting that contact tracing alone is unable to eradicate a disease.

The literature proposes a variety of modelling choices to represent the effects of contact tracing, and these choices can influence whether the intervention contributes to the epidemic threshold or not. For instance, in de Meijere and Castellano (2023), traced individuals are defined as those infected by a contact tracing–triggering node. When, as per this modelling choice, contact tracing depends on the pairwise interaction between susceptible and infected individuals, the linear stability analysis no longer cancels the contribution of contact tracing to the epidemic threshold.

C Numerical threshold

The epidemic threshold can be studied numerically in two different ways: through the final epidemic size or the initial growth rate of the epidemic.

Final epidemic size. In terms of the final epidemic size, the epidemic threshold is the lowest value of c_p for which a nonzero final size can be reached from an infinitesimal initial condition. In Fig. 6a, we show the final epidemic size, or the stationary number of recovered individuals R_∞ as a function of the initial number of infected individuals $[I](t=0)$, for various values of the contact tracing rate c_p. We consider values of c_p that span the surroundings of the threshold value c_p^* which has been computed analytically using the approximate fast variables method [Eq. (3.8)].

Regardless of how small the initial condition is, the final epidemic size is always non-zero, making the numerical threshold blurry. Nevertheless, fitting a line through the final epidemic sizes as functions of the initial conditions, we can estimate the final epidemic size in the limit of a zero initial condition $[I](0)/N \to 0$. In this limit, we see that the analytical threshold is a good estimate of the numerical threshold, separating a regime where c_p is large and the final epidemic size is zero from a regime where c_p is small and the final epidemic size is non-zero.

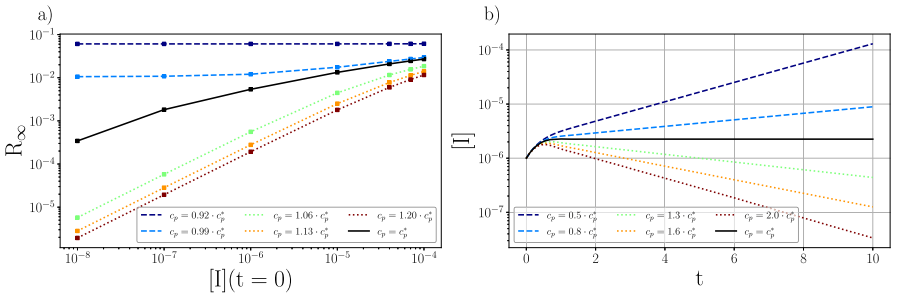


Fig. 6 Numerical threshold in the pure pairwise contact tracing. **a** The final epidemic size R_∞ as a function of the initial condition $I(0)$ for different values of the tracing parameter c_p. **b** The time dependence of the prevalence $[I]$ for different values of the contact tracing rate c_p with initial condition $I(0) = 10^{-6}$. Parameter values: $n = 5$, $a = 1$, $q = 0.6$, and $c_t = 0$

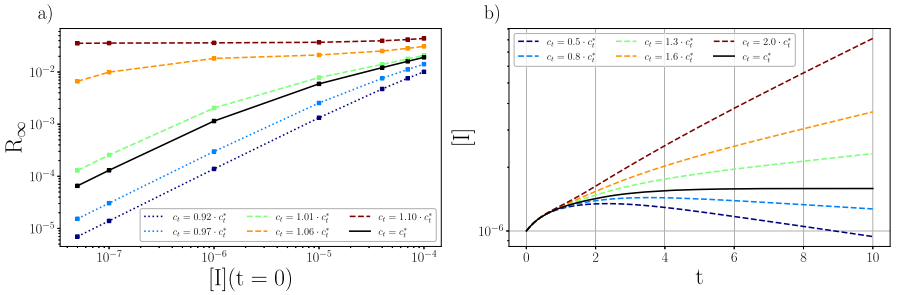


Fig. 7 Numerical threshold in the pure triplewise contact tracing. **a** The final epidemic size R_∞ as a function of the initial condition $I(0)$ for different values of the tracing parameter c_t. **b** The time dependence of the prevalence $[I]$ for different values of the contact tracing rate c_t with initial condition $I(0) = 10^{-6}$. Parameter values: $n = 5$, $\tau = 0.18$, $a = 0.6$, $q = 0.6$, and $c_p = 0$

Initial growth rate. Concerning the initial growth rate of the epidemic prevalence, the contact tracing parameter c_p plays a slightly delayed role. In Fig. 6b, we show the time evolution of the prevalence for three values of c_p in the neighborhood of the analytical threshold value c_p^*. We find that although the different choices of c_p do not affect the initial growth, after some initial transient time, the contact tracing measure finally kicks in and the role of c_p becomes visible. This transient time happens to also be the time for the fast variables to reach their steady-state. As soon as the fast variables have stabilized, c_p exhibits the following influence: at the threshold value $c_p = c_p^*$ [Eq. (3.8)] the prevalence stabilizes to a constant value, when $c_p > c_p^*$ the prevalence is exponentially suppressed, and when $c_p < c_p^*$ it grows exponentially fast.

The corresponding figures for pure triplewise contact tracing are provided in Fig. 7.

D Derivation of the critical level of pure pairwise contact tracing

In this section, we show the main steps of the derivation of the critical level of pure pairwise contact tracing.

Let's consider Eq. (3.7), with $c_t = 0$ (pure pairwise):

$$\begin{cases} \tau x - 1 - c_p^* z = 0 \\ \tau x(n-2) - c_p^* \frac{(n-1)}{n} xz - x = 0 \\ 2\tau x - 2y - 2c_p^* \frac{(n-1)}{n} yz = 0 \\ -az + c_p^* \left(\frac{(n-1)}{n} yz - \frac{(n-1)}{n} z^2 - z \right) + (qy - z) = 0. \end{cases} \tag{D.1}$$

In the second equation, we readily see that x factorizes, while the factor 2 simplifies across the third equation. Let $R_0 := \tau(n-2)$ be the basic reproductive number (note that τ is the ratio between the infection rate and the total recovery rate), and $\kappa := \frac{(n-1)}{n}$. Then Eq. (D.1) becomes:

$$\begin{cases} \tau x - 1 - c_p^* z = 0 \\ R_0 - c_p^* \kappa z - 1 = 0 \\ \tau x - y - c_p^* \kappa yz = 0 \\ -az + c_p^* \left(\kappa yz - \kappa z^2 - z \right) + qy - z = 0. \end{cases} \tag{D.2}$$

The second equation allows one to express z as a function of the model parameters:

$$z = \xi \cdot \frac{1}{c_p^*}, \tag{D.3}$$

where $\xi = \frac{R_0 - 1}{\kappa}$. Note that z depends on the contact tracing parameter c_p^*.

Plugging this in the first equation of Eq. (D.2), we can then also express x as a function of the model parameters only:

$$\tau x = 1 + \xi. \tag{D.4}$$

Using the third equation of Eq. (D.2), and plugging the expressions for x and z derived in Eq. (D.4) and Eq. (D.3), we can finally also express y as a function of the model parameters:

$$y = \frac{1}{R_0} \left(1 + \frac{R_0 - 1}{\kappa} \right) = \frac{1}{R_0} \cdot (1 + \xi). \tag{D.5}$$

Ultimately, the fourth equation of Eq. (D.2) can be used to express the pure pairwise contact tracing rate c_p^* as a function of the fast variables x, y and z, and the model parameters. Plugging the expressions of the fast variables in terms of the model parameters [Eq. (D.4), Eq. (D.5), and Eq. (D.3)], we get:

$$-a \frac{\xi}{c_p^*} + \frac{\kappa}{R_0}(1 + \xi)\xi - \kappa \xi^2 \frac{1}{c_p^*} - \xi + \frac{q}{R_0}(1 + \xi) - \xi \frac{1}{c_p^*} = 0 \tag{D.6}$$

$$c_p^* = \frac{R_0\xi(a+1+\kappa\xi)}{(1+\xi)(\kappa\xi+q) - R_0\xi} \tag{D.7}$$

$$= (a+R_0)\,\frac{R_0-1}{F_p(n,q,\tau)}, \tag{D.8}$$

where $F_p(n,q,\tau) = \frac{1}{n}\frac{R_0(nq-1)+(1-q)}{R_0}$.

E Derivation of the critical level of pure triplewise contact tracing

In this section, we show the main steps of the derivation of the critical level of pure triplewise contact tracing.

Let's consider Eq. (3.7), with $c_p = 0$ (pure triplewise):

$$\begin{cases} \tau x - 1 - c_t^* \frac{(n-1)}{n} z^2 = 0 \\ \tau(n-2) - c_t^* \frac{(n-1)(n-2)}{n^2} z^2 - 1 = 0 \\ \tau x - y - c_t^* \frac{(n-1)(n-2)}{n^2} y z^2 = 0 \\ -az + c_t^* z^2 \left(\frac{(n-1)(n-2)}{n^2} y - \frac{(n-1)}{n} - \frac{(n-1)(n-2)}{n^2} z \right) + (qy - z) = 0. \end{cases} \tag{E.1}$$

Let $R_0 := \tau(n-2)$ be the basic reproductive number, $\kappa := \frac{(n-1)}{n}$, and $\hat{\kappa} := \frac{(n-1)(n-2)}{n^2}$. Then Eq. (E.1) becomes:

$$\begin{cases} \tau x - 1 - c_t^* \kappa z^2 = 0 \\ R_0 - c_t^* \hat{\kappa} z^2 - 1 = 0 \\ \tau x - y - c_t^* \hat{\kappa} y z^2 = 0 \\ -az + c_t^* z^2 \left(\hat{\kappa} y - \kappa - \hat{\kappa} z \right) + qy - z = 0. \end{cases} \tag{E.2}$$

The second equation allows one to express z^2 as a function of the model parameters:

$$z^2 = \frac{\xi}{\kappa} \cdot \frac{1}{c_t^*}, \tag{E.3}$$

where $\xi = \kappa \frac{R_0-1}{\hat{\kappa}}$. Note that z^2 depends on the contact tracing parameter c_t^*.

Plugging this in the first equation of Eq. (E.2), we can then also express x as a function of the model parameters only:

$$\tau x = 1 + \xi. \tag{E.4}$$

Using the third equation of Eq. (E.2), and plugging the expressions for x and z^2 derived in Eq. (E.4) and Eq. (E.3), we can finally also express y as a function of the

model parameters:

$$y = \frac{1}{R_0} \cdot (1 + \xi). \tag{E.5}$$

Ultimately, the fourth equation of Eq. (E.2) can be used to express the pure triple-wise contact tracing rate c_t^* as a function of the fast variables x, y and z, and the model parameters. Plugging the expressions of the fast variables in terms of the model parameters [Eq. (E.4), Eq. (E.5), and Eq. (E.3)], we get:

$$-z(a + 1 + R_0 - 1) + q\frac{1+\xi}{R_0} + \frac{\xi}{\kappa}(\hat{\kappa}\frac{1+\xi}{R_0} - \kappa) = 0 \tag{E.6}$$

$$\frac{1}{z} = \frac{(a + R_0)}{q\frac{1+\xi}{R_0} + \frac{R_0-1}{R_0}(1+\xi) - \xi} \tag{E.7}$$

$$\begin{aligned} c_t^* &= \frac{(a + R_0)^2}{(q\frac{1+\xi}{R_0} + \frac{R_0-1}{R_0}(1+\xi) - \xi)^2}\frac{\xi}{\kappa} = \frac{(a + R_0)^2(R_0 - 1)}{\hat{\kappa}(q\frac{1+\xi}{R_0} + \frac{R_0-1}{R_0}(1+\xi) - \xi)^2} \\ &= (a + R_0)^2 \frac{R_0 - 1}{F_t(n, q, \tau)}, \end{aligned} \tag{E.8}$$

where $F_t(n, q, \tau) = \frac{(n-1)}{n^2(n-2)}\left(\frac{R_0(nq-2)+2(1-q)}{R_0}\right)^2$.

References

Ball F, Britton T, House T, Isham V, Mollison D, Pellis L, Tomba GS (2015) Seven challenges for metapopulation models of epidemics, including households models. Epidemics 10:63–67

Barnard RC, Berthouze L, Simon PL, Kiss IZ (2019) Epidemic threshold in pairwise models for clustered networks: closures and fast correlations. J Math Biol 79:823–860

Barrat A, Cattuto C, Kivelä M, Lehmann S, Saramäki J (2021) Effect of manual and digital contact tracing on covid-19 outbreaks: a study on empirical contact data. J R Soc Interface 178:18

Bradshaw WJ, Alley EC, Huggins JH, Lloyd AL, Esvelt KM (2021) Bidirectional contact tracing could dramatically improve COVID-19 control. Nat Commun 12(1):232

Brandt AM, The History of Contact Tracing and the Future of Public Health, Am J Public Health (2022), https://doi.org/10.2105/AJPH.2022.306949

Britton T, Juher D, Saldaña J (2016) A network epidemic model with preventive rewiring: comparative analysis of the initial phase. Bull Math Biol 78(12):2427–2454

Chowell GMAM, Miller MA, Viboud C (2008) Seasonal influenza in the United States, France, and Australia: transmission and prospects for control. Epidemiol Infect 136(6):852–864

Davis EL, Lucas TCD, Borlase A, Pollington TM, Abbott S, Ayabina D, Crellen T, Hellewell J, Pi L, Medley GF et al (2021) Contact tracing is an imperfect tool for controlling COVID-19 transmission and relies on population adherence. Nat Commun 12(1):5412

de Meijere G, Castellano C (2023) Limited efficacy of forward contact tracing in epidemics. Phys Rev E 108(5):054305

de Meijere G, Valdano E, Castellano C, Debin M, Kengne-Kuetche C, Turbelin C, Noël H, Weitz JS, Paolotti D, Hermans L et al (2023) Attitudes towards booster, testing and isolation, and their impact on covid-19 response in winter 2022/2023 in france, belgium, and italy: a cross-sectional survey and modelling study. The Lancet Regional Health-Europe 28:100614

Di Domenico L, Pullano G, Sabbatini CE, Boëlle P-Y, Colizza V (2020) Impact of lockdown on COVID-19 epidemic in Île-de-France and possible exit strategies. BMC Med 18(1):240

Eames KTD, Keeling MJ (2003) Contact tracing and disease control. In: Proceedings of the Royal Society of London. Series B: Biological Sciences 270(1533):2565–2571
Ferretti L, Wymant C, Kendall M, Zhao L, Nurtay A, Abeler-Dörner L, Parker M, Bonsall D, Fraser C (2020) Quantifying SARS-CoV-2 transmission suggests epidemic control with digital contact tracing. Science 368(6491):eabb6936
Fraser C, Riley S, Anderson RM, Ferguson NM (2004) Factors that make an infectious disease outbreak controllable. Proc Natl Acad Sci 101(16):6146–6151
George W, Rutherford JM, Woo, (1988) Contact tracing and the control of human immunodeficiency virus infection. JAMA 259(24):3609–3610
Hellewell J, Abbott S, Gimma A, Bosse NI, Jarvis CI, Russell TW, Munday JD, Kucharski AJ, John Edmunds W, Funk S et al (2020) Feasibility of controlling COVID-19 outbreaks by isolation of cases and contacts. Lancet Glob Health 8(4):e488–e496
Holme P, Saramäki J (2012) Temporal networks. Phys Rep 519(3):97–125
Hossain AD, Jarolimova J, Elnaiem A, Huang CX, Richterman A, Ivers LC (2022) Effectiveness of contact tracing in the control of infectious diseases: a systematic review. The Lancet Public Health 7(3):e259–e273
House T, Keeling MJ (2010) The impact of contact tracing in clustered populations. PLoS Comput Biol 6(3):e1000721
House T, Davies G, Danon L, Keeling MJ (2009) A motif-based approach to network epidemics. Bull Math Biol 71(7):1693–1706
István Z Kiss JC, Miller PL, Simon (2017) Mathematics of epidemics on networks: from exact to approximate models. Interdiscip Appl Math 46
Keeling MJ (1999) The effects of local spatial structure on epidemiological invasions. In: Proceedings of the Royal Society of London. Series B: Biological Sciences 266(1421):859–867
Keeling MJ, Eames KTD (2005) Networks and epidemic models. J R Soc Interface 2(4):295–307
Kermack WO, McKendrick AG (1927) A contribution to the mathematical theory of epidemics. Proc R Soc Lond A 115(772):700–721
Kivelä M, Arenas A, Barthelemy M, Gleeson JP, Moreno Y, Porter MA (2014) Multilayer networks. J Complex Networks 2(3):203–271
Kojaku S, Hébert-Dufresne L, Mones E, Lehmann S, Ahn Y-Y (2021) The effectiveness of backward contact tracing in networks. Nat Phys 17(6):652–658
Mancastroppa M, Castellano C, Vezzani A, Burioni R (2021) Stochastic sampling effects favor manual over digital contact tracing. Nat Commun 12(1):1919
Mettler SK, Park J, Özbek O, Mettler LK, Ho P-H, Rhim HC, Maathuis MH (2021) The importance of timely contact tracing-a simulation study. Int J Infect Dis 108:309–319
Miller JC (2011) A note on a paper by Erik Volz: SIR dynamics in random networks. J Math Biol 62(3):349–358
Moreno JA, López BA, García PB, Bioglio L, Pinotti F, Boëlle P-Y, Barrat A, Colizza V, Poletto C (2021) Anatomy of digital contact tracing: role of age, transmission setting, adoption, and case detection. Sci Adv 7(15):eabd8750
Müller J, Kretzschmar M (2021) Contact tracing-old models and new challenges. Infect Disease Model 6:222–231
Newman MEJ (2018) Networks. Oxford University Press, Oxford
Pastor-Satorras R, Castellano C, Van Mieghem P, Vespignani A (2015) Epidemic processes in complex networks. Rev Mod Phys 87(3):925–979
Pellis L, Ball F, Bansal S, Eames K, House T, Isham V, Trapman P (2015) Systematic selection between age and household structure for models aimed at emerging epidemic predictions. Nat Commun 6(1):7261
Peralta AF, Kertész J, Iñiguez G (2025) Opinion dynamics in social networks: from models to data. In: Taha Yasseri (ed) Handbook of Computational Social Science, Edward Elgar Publishing Limited, pp 384–406
Starnini M, Baumann F, Galla T, Garcia D, Iñiguez G, Karsai M, Lorenz J, Katarzyna Sznajd-Weron (2025) Opinion dynamics: statistical physics and beyond. Rev. Mod. Phys. (2006), https://doi.org/10.1103/j1zg-ddqv
Stephenson JF (2023) Sharing fluids shapes host social networks and pathogen traits. In: Proceedings of the Royal Society B: Biological Sciences 290(2000)

Trentini F, Pariani E, Bella A, Diurno G, Crottogini L, Rizzo C, Merler S, Ajelli M (2022) Characterizing the transmission patterns of seasonal influenza in Italy: lessons from the last decade. BMC Public Health 22(1):19

Unicomb S, Iñiguez G, Gleeson JP, Karsai M (2021) Dynamics of cascades on burstiness-controlled temporal networks. Nat Commun 12(1):133

Ureña-Carrion J, Heydari S, Aledavood T, Saramäki J, Kivelä M (2026) Multiplexity is temporal: effect of social times on network structure. EPJ Data Sci 15(1):11

Zhang D, Britton T (2024) An SEIR network epidemic model with manual and digital contact tracing allowing delays. Math Biosci 374:109231

Zhang D, Favero M (2025) Sideward contact tracing in an epidemic model with mixing groups. Methodol Comput Appl Probab 27(2):33

Publisher's Note Springer Nature remains neutral with regard to jurisdictional claims in published maps and institutional affiliations.